




Doppler Factor Estimation for Fermi Blazars

Lixia Zhang^{1,2,3}, Sina Chen^{1,4,5}, Hubing Xiao^{1,4,5} , Jinting Cai^{1,2,3}, and Junhui Fan^{1,2,3}

¹Center for Astrophysics, Guangzhou University, Guangzhou 510006, People's Republic of China; fjh@gzhu.edu.cn

²Astronomy Science and Technology Research Laboratory of Department of Education of Guangdong Province, Guangzhou, 510006, People's Republic of China

³Key Laboratory for Astronomical Observation and Technology of Guangzhou, Guangzhou 510006, People's Republic of China

⁴Department of Physics and Astronomy "G. Galilei," University of Padova, Padova, Italy

⁵Istituto Nazionale di Fisica Nucleare, Sezione di Padova, Padova, Italy

Received 2020 January 27; revised 2020 April 26; accepted 2020 May 5; published 2020 June 26

Abstract

In this work, we exploit the luminosity of the broad-line region (BLR) for 50 Fermi blazars through matching the coordinates between the Sloan Digital Sky Survey catalog, Fermi Large Area Telescope Third Source Catalog, and the Fermi Large Area Telescope Fourth Source Catalog and fitting their emission lines. In total, we collected a sample of 350 blazars with broad-line emissions including 50 new objects and 300 blazars from published works to revisit the correlation between the γ -ray luminosity and the broad-line luminosity, and proposed a new method to estimate the Doppler factors based on the correlation between the radiative power of the jet and luminosity of the BLR. We come to following conclusions. (1) For the 50 Fermi blazars, their broad-line luminosity ($\log L_{\text{BLR}}$) ranges from 41.82–45.2 erg s^{-1} with a mean value of 44.39 erg s^{-1} . (2) The Doppler factor (δ) ranges from $\delta = 0.35$ to $\delta = 85.66$ with a mean value of 12.54, which is consistent with the results in the literature. (3) There are positive correlations between γ -ray luminosity and broad-line luminosity, and between γ -ray luminosity and the Doppler factor.

Unified Astronomy Thesaurus concepts: Active galactic nuclei (16); Blazars (164); High energy astrophysics (739); Jets (870)

Supporting material: machine-readable tables

1. Introduction

As the most powerful class of active galactic nuclei (AGNs), blazars are characterized by extreme observation properties, such as high luminosity, large and rapid variability, high and variable polarization, superluminal radio components, a core-dominated nonthermal continuum, and bright γ -ray emission, etc. (Abdo et al. 2010a, 2010b; Acero et al. 2015; Ackermann et al. 2015; Fan et al. 2016, 2017, 2018). A beaming model was proposed to be responsible for these special properties, within the model there is a supermassive black hole at the center, surrounded by an accretion disk with jets coming out from the center at directions perpendicular to the accretion disk. In this model, the jet is close to our line of sight and results in a beaming boosting effect (Blandford & Rees 1978; Urry & Padovani 1995). The beaming factor (or Doppler factor) is determined by the viewing angle (θ), coupled with the velocity of the jet (β): $\delta = [\Gamma(1 - \beta \cos \theta)]^{-1}$, where $\Gamma = 1/\sqrt{1 - \beta^2}$ is the Lorentz factor. Based on the behavior of emission lines, blazars can be divided into two subclasses: flat-spectrum radio quasars (FSRQs) with strong emission lines, and BL Lacertae (BL Lac) objects with weak or absent ones.

Since it is notoriously difficult to obtain the Doppler factors, δ , some indirect methods are proposed for their estimation: mostly from the mechanism of synchrotron self-Compton (SSC) using very long baseline interferometry observations and X-ray flux density to achieve δ_{SSC} (Ghisellini et al. 1993), from the rapid γ -ray variability timescale, X-ray, and γ -ray emissions (Mattox et al. 1993; von Montigny et al. 1995; Cheng et al. 1999; Fan et al. 1999, 2009, 2013, 2014; Fan 2005), or from radio flux density variations to access δ_{var} (Lähteenmäki & Valtaoja 1999). In a recent work, Lioudakis et al. (2018) proposed that the variability Doppler factors can

be computed by constraining the equipartition brightness temperature, and obtained variability Doppler factors for a sample of 837 blazars. Meanwhile, Chen (2018) estimated the Doppler factors based on broadband spectral energy distributions (SEDs) for a sample of 999 blazars.

For the beaming model, both jet and accretion are important. The relation between the jet and the accretion process plays an important role in the understanding of the central engine inside AGNs. It is generally believed that the jet is generated from a spinning black hole (Blandford & Znajek 1977), or from the accretion disk (Blandford & Payne 1982), while the magnetic field serves as a medium for energy transfer from the center of the black hole or accretion disk to jets (Maraschi & Tavecchio 2003). The relationship of jet power with accretion luminosity will be expected if the square magnetic field varies directly with the accretion rate (Ghisellini et al. 2014). However, the jet power and accretion emission are hard to detect directly, so many authors explored such a relationship from observable quantities (Celotti et al. 1997; Cao & Jiang 1999; Sbarrato et al. 2012; Ghisellini et al. 2014; Xiong & Zhang 2014). The luminosity of the broad-line region (BLR) can represent the accretion emission, since it is produced by the gas in the BLR photoionized by the radiation from accretion disk (Kaspi et al. 2000, 2005; Bentz et al. 2009; Sbarrato et al. 2012). The jet cannot transport its entire power into radiation that is detected by instruments, otherwise the jet will stop. From this aspect, the radiative power of the jet is a lower limit

on the jet power $P_{\text{jet}} > P_{\text{rad}} > \frac{L_{\text{jet}}^{\text{bol}}}{\Gamma^2}$, where $L_{\text{jet}}^{\text{bol}}$ is the jet bolometric luminosity and Γ is the Lorentz factor (Sbarrato et al. 2012). In the scenario of γ -ray loud blazars, the bolometric luminosity is dominated by γ -ray luminosity, and the γ -ray luminosity often takes the place of bolometric luminosity in previous research (Ghisellini et al. 2014;

Xiong & Zhang 2014). Thus, the γ -ray emissions of a large number of blazars detected from the Fermi Large Area Telescope (LAT) can provide a good estimation for the radiative power of the jet, as a lower limit to the jet power.

From the multiwavelength observations of blazars, the SED shows a bimodal shape from the synchrotron radiation of relativistic electrons in the jet (Urry 1998); the low-energy component of the SED has peak frequencies ranging from infrared to optical or even to the X-ray band. The high-energy component with peak frequencies from mega- to teraelectronvolts, however, is controversial with the radiation mechanism. The main mechanisms for the origin of γ -ray emissions are as follows. One mechanism is the SSC model, here they may be caused by the same electron-emitting synchrotron radiation as inverse Compton (IC) emission, where the seed photons are provided by the synchrotron emission (Maraschi et al. 1992; Dermer & Schlickeiser 1993; Sikora et al. 1994; Bloom & Marscher 1996), or by external Compton (EC) emission where the seed photons come from the accretion disk (Dermer & Schlickeiser 1993), torus (Blażejowski et al. 2000), or the BLR (Fan et al. 2006). The other mechanism is a hadronic model, where γ -ray emissions may be produced by radiation from the synchrotron of relativistic protons, the cascade process of photons and mesons, and the synchrotron radiation of mesons (Aharonian 2000, 2002). Consensus has not been reached on the dominant emission process. Generally, because BL Lac objects lack strong emission lines, then the radiation such as the EC component from the BLR is reduced, and the SSC component quite possibly becomes the emission process (Doni & Ghisellini 1995). Chen (2018) also pointed that the γ -ray emission of BL Lac objects is attributed to the SSC emission because of the weak or absent emission lines, while that of FSRQs with strong emission lines is attributed to the EC emission.

From this physical point of view, Ghisellini et al. (2014) measured jet power and accretion disk luminosity from γ -ray luminosity and broad-line luminosity, respectively, and obtained a correlation between jet power and accretion disk luminosity: $\log P_{\text{rad}} \sim 0.98 \log L_{\text{disk}} + 0.639$, here $P_{\text{rad}} = 2fL_{\text{jet}}^{\text{bol}}/\delta^2$, where the factor of 2 indicates two jets and f is a constant ($f = 4/3$ for the case of the SSC component with isotropic emission and $f = 16/5$ for the case of anisotropic emission dominated by the EC component, see Ghisellini & Tavecchio (2010) for details). The result is in agreement with the theoretical prediction. Thus the correlation between jet power and accretion disk luminosity can be converted into one between γ -ray luminosity and broad-line luminosity. In the case of blazars, the viewing angle is small, $\sin(\theta) \approx 1/\Gamma$, so $\delta \approx \Gamma$, this correlation then provides a method to evaluate the Doppler factor.

From the available works on the correlation between the jet and the accretion, there are a total of 300 Fermi blazars with emission lines (Ghisellini et al. 2014; Xiong & Zhang 2014). The aim of this work is to enlarge the sample of Fermi blazars showing emission lines by cross-matching the catalogs with the Sloan Digital Sky Survey (SDSS; York et al. 2000) with the Fermi Large Area Telescope Third and Fourth Source Catalogs (3FGL and 4FGL) to revisit the correlation between γ -ray luminosity and the broad-line luminosity and to estimate the Doppler factor. The work is arranged as follows: the matching sample is presented in Section 2, the Doppler factor estimation is in Section 3, and the discussions and conclusions are in

Sections 4 and 5. Throughout this paper, the cosmology constant is adopted by the Λ CDM model with $H_0 = 71 \text{ km s}^{-1} \text{ Mpc}^{-1}$, $\Omega_{\Lambda} = 0.73$, $\Omega_{\text{M}} = 0.27$ (Komatsu et al. 2011).

2. Sample

Our sample consists of two parts: one part is obtained from the literature, which is the initial sample with available broad-line luminosity, the other part is derived from the matching result. The initial blazar sample is from Ghisellini et al. (2014) and Xiong & Zhang (2014). There are 217 sources with available emission-line luminosities in each of the two samples (Ghisellini et al. 2014; Xiong & Zhang 2014), however there are 134 common sources in the two samples. As a consequence, we have 300 blazars in total with broad-line emissions. In the work by Ghisellini et al. (2014), the logarithm of the disk luminosity calculated from broad-line luminosity for each source is given, while in the work of Xiong & Zhang (2014), the broad-line luminosity was from the literature: Cao & Jiang (1999), Sbarrato et al. (2012), Shaw et al. (2012), Chai et al. (2012), Shen et al. (2011), Liu et al. (2006), and Wang et al. (2004). In the present work, we will expand the sample by matching 3FGL and 4FGL with SDSS within 0'.5. The selection process is that if a source in SDSS matches a source in 3FGL or 4FGL, then we check whether the source appeared in the listed works. If the source was not included in the literature, then we obtain its emission-line information from SDSS for further analysis. In this way, we got 50 new sources (48 FSRQs and two BL Lac objects) with the peak of broad emission lines greater than or equal to three times rms.

This finally leads to a sample of 350 blazars (75 BL Lac objects and 275 FSRQs). Among the 350 sources, 26 objects (four from SDSS and 22 from published results) are not included in the 4FGL. Eighteen out of the 26 objects were included in 3FGL (Acero et al. 2015), one in the Fermi Large Area Telescope Second Source Catalog (2FGL) and seven in the Fermi Large Area Telescope First Source Catalog (1FGL; see Abdo et al. 2010a; Xiong & Zhang 2014). These are listed in Table 1. Among the published results, we took the values from Xiong & Zhang (2014) for the common sources appearing in the two works (Ghisellini et al. 2014; Xiong & Zhang 2014). The redshift is distributed in a range of 0.03–3.104 with a mean value of 1.153. The average values are $z = 1.217$ for FSRQs and $z = 0.921$ for BL Lac objects.

2.1. Broad-line Luminosity of 50 Blazars

As explained in a paper by Chen et al. (2018), the spectra of 50 new blazars are from the SDSS archive. For each source, the redshift correction was performed first, then the magnitude was corrected for galactic extinction by A_{λ} coefficients (Schlafly & Finkbeiner 2011) from the NASA/IPAC Extragalactic Database. The continuum was fitted by a power-law in the continuum region in four wavelength intervals (1700–1800 Å, 2950–3050 Å, 5050–5150 Å, and 6700–6800 Å), where there are no strong emission lines, subsequently, the continuum was subtracted from the original spectra. The rms was computed in the wavelength intervals mentioned above. The emission line was identified based on the criterion that the peak of emission line is not less than 3 rms, and each of them was fitted by Gaussians. The signal-to-noise ratio (S/N) was also calculated in the wavelength intervals mentioned above, and each emission line was fitted by three Gaussians (S/N > 10), two

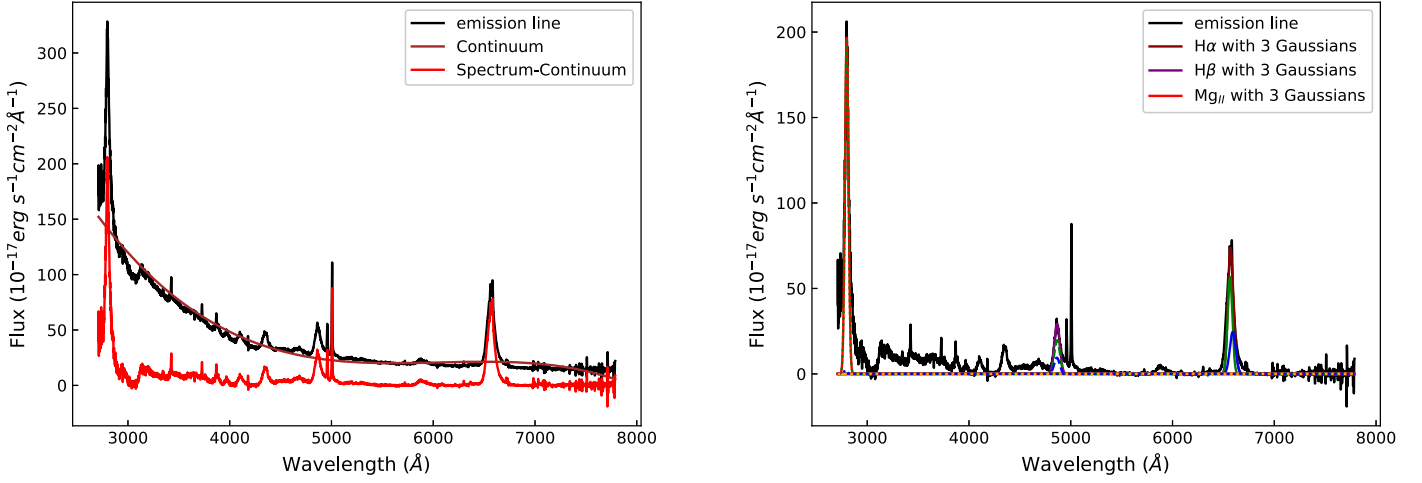


Figure 1. Left panel: an example shows a power-law fitting for the continuum of 4FGL J1153.4+4931, the black solid line is the original spectrum, the brown solid line is the continuum, the red solid line is the one that subtracts the continuum from the original spectrum. Right panel: an example shows the Gaussian fit for the BLR emissions of 4FGL J1153.4+4931, the black solid line is for $H\alpha$, the purple solid line is for $H\beta$, the crimson solid line is for C_{IV} , and the red solid line is for Mg_{II} . If there are three components for the emission line, green is the narrow one, blue is the broad one and orange is the most broad one. If there are two components for the emission line, green is the narrow one and blue is the broad one.

Table 1
Sample for Blazars

Name (1)	Other Name (2)	z (3)	Classification (4)	F_{1-100} (5)	α_{ph} (6)	$\log L_\gamma$ (7)	$\log L_{BLR}$ (8)	References (9)	δ (10)
4FGL J0004.4–4737	PKS 0002–478	0.880	CF	4.86E–10	2.42	46.03	44.11	Sh12	10.82
4FGL J0011.4+0057	[VV2006] J001130.4+005751	1.493	CB	4.75E–10	2.32	46.64	44.60	G14	6.13
4FGL J0014.1+1910	ICRF J001356.3+191041	0.477	CB	1.94E–10	2.26	44.97	42.70	G14	5.99
4FGL J0016.5+1702	0015+1700	1.709	CB	1.77E–10	2.63	46.39	45.26	G14	2.36
4FGL J0016.2–0016	S3 0013–00	1.574	CF	4.76E–10	2.73	46.73	44.91	S11	8.21
4FGL J0017.5–0514	PMN 0017–0512	0.227	CF	8.69E–10	2.53	44.76	43.79	Sh12	3.89

Note. Column definitions: (1) name; (2) other name; (3) redshift (z); (4) classification: “CF” and “CB” are the confirmed FSRQs and confirmed BL Lac objects. “UF” and “UB” are the uncertain type BCUs (blazars of uncertain type) classified as FSRQs and BL Lac objects, respectively; (5) γ -ray photons in $1 \sim 100$ GeV in units of photon $\text{cm}^{-2} \text{s}^{-1}$ (F_{1-100}); (6) the photon spectral index from power-law fitting (α_{ph}); (7) logarithm of the γ -ray luminosity ($1 \sim 100$ GeV) in units of erg s^{-1} ($\log L_\gamma$); (8) logarithm of the broad-line region luminosity in units of erg s^{-1} ($\log L_{BLR}$); (9) references for (8): C99: Cao & Jiang (1999); C12: Chai et al. (2012); L06: Liu et al. (2006); Sb12: Sbarrato et al. (2012); Sh12: Shaw et al. (2012); S11: Shen et al. (2011); W04: Wang et al. (2004); G14: Ghisellini et al. (2014); TW: broad-line region luminosity calculated in this work for the 50 new sources; (10) Doppler factor obtained in this work, δ .

(This table is available in its entirety in machine-readable form.)

Gaussians ($1 < S/N < 10$), or one Gaussian ($S/N < 1$). The flux of the emission line was integrated along the fitted profile, and the corresponding luminosity of the emission line was obtained from the integrated flux: $L_{BLR} = 4\pi d_L^2 \lambda F(\lambda)$, where $d_L = (1+z) \cdot \frac{c}{H_0} \cdot \int_1^{1+z} \frac{1}{\sqrt{\Omega_M x^3 + 1 - \Omega_M}} dx$ is luminosity distance from the Λ CDM model (Capelo & Natarajan 2007), and $\lambda F(\lambda)$ is the flux density in units of $\text{erg s}^{-1} \text{cm}^{-2} \text{\AA}^{-1}$. The procedures mentioned above are implemented by python. As an example, the continuum fitting and emission lines fitting are shown in the left and right panels of Figure 1.

The normalization is applied to the total broad-line luminosity (Celotti et al. 1997): $L_{BLR} = \sum_i L_{i,obs} \frac{\langle L_{BLR}^* \rangle}{\sum_i L_{i,est}^*}$, where $\sum_i L_{i,obs}$ is the total observed luminosities obtained from a certain number of broad lines, $\sum_i L_{i,est}^*$ is the total luminosities obtained from the same lines, and estimated from the line ratios which is adopted, and $\langle L_{BLR}^* \rangle$ is the total luminosities of the same lines reported in Francis et al. (1991). Here we take $\langle L_{BLR}^* \rangle = 5.56 L_{y\alpha}^*$, and set $L_{y\alpha}^* = 100$. Since the $H\alpha$, $H\beta$, Mg_{II} , and C_{IV} lines have a significant contribution to the major parts

of the total broad-line emissions, their weights were set to be 77, 22, 34, and 63, respectively (Francis et al. 1991; Sbarrato et al. 2012). When there are two or more emission lines for a source, we will use the average value as the broad-line luminosity. For the 50 new Fermi blazars, the logarithm of the broad-line luminosity, $\log L_{BLR}$ (erg s^{-1}), listed in column (8) in Table 1 and shown in Figure 2, is in a range of 41.82–45.2 with a mean value of 44.39. Also in Table 1, we listed the emission-line luminosity of the other 300 sources from the literature.

3. Results

3.1. Correlation between γ -Ray Luminosity and the Broad-line Luminosity

From the Fermi/LAT catalog, we can calculate the γ -ray luminosity using the γ -ray photons, the photon spectral index, and the redshift for each γ -ray source as $L_\gamma = 4\pi d_L^2 (1+z)^{(\alpha_{ph}-2)} F$, where z is redshift, $(1+z)^{(\alpha_{ph}-2)}$ is a K -correction, α_{ph} is the photon spectral index, and F is the integral flux in units of $\text{GeV cm}^{-2} \text{s}^{-1}$, see Fan et al. (2016)

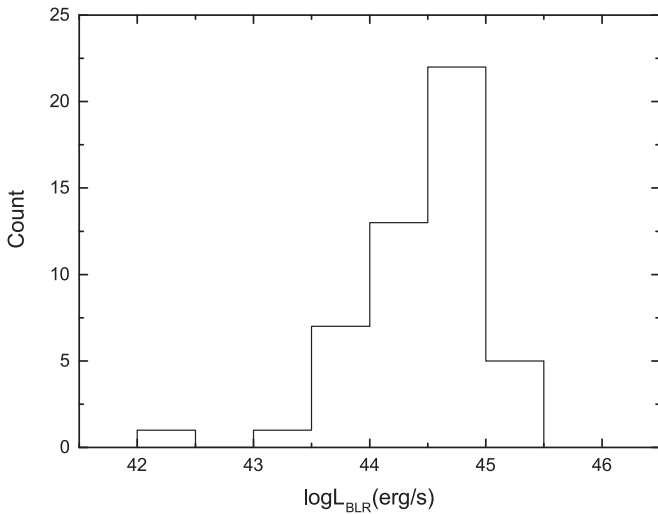


Figure 2. Distributions for the logarithm of the BLR luminosity for 50 blazars from our calculation.

and references therein for details. The γ -ray photons and photon spectral indexes of 324 sources in the 4FGL (The Fermi-LAT Collaboration 2019), those of 18 sources in the 3FGL, that of one source in the 2FGL, and those of seven sources in the 1FGL are employed for the γ -ray luminosity calculations in the range of 1 \sim 100 GeV. The logarithm of the γ -ray luminosity is listed in column (7) in Table 1. When a linear regression analysis method of ordinary and symmetrical least-squares regression (OLS)⁶ (Feigelson & Babu 1992) is performed to the γ -ray luminosity and the broad-line luminosity of sources, we have the OLS bisector

$$\log L_{\gamma} = (1.11 \pm 0.04) \log L_{\text{BLR}} - (3.00 \pm 1.82)$$

with a correlation coefficient of $r = 0.62$ and a chance probability of $p < 0.0001$ for the 350 blazars. The corresponding result is shown in Figure 3 and listed in Table 2.

3.2. Estimation of the Doppler Factor

According to Ghisellini et al. (2014), the viewing angle of blazars is small, $\sin(\theta) \approx 1/\Gamma$, so $\delta \approx \Gamma$. The nonthermal radiation supplied by a jet is

$$P_{\text{rad}} = 2fL_{\text{jet}}^{\text{bol}} / \delta^2, \quad (1)$$

where the factor of 2 indicates two jets, and f is a constant ($f = 4/3$ for BL Lac objects (dominated by SSC), and $f = 16/5$ for FSRQs (dominated by EC)). Ghisellini et al. (2014) obtained a close linear correlation for the nonthermal radiation and the disk luminosity by least-squares best fit, $\log P_{\text{rad}} \sim 0.98 \log L_{\text{disk}} + 0.639$ for a sample of 217 blazars.

If we considered BL Lac objects and FSRQs in Ghisellini et al. (2014) separately with the linear regression analysis method of OLS, we have

$$\log P_{\text{rad}} = 1.178 \log L_{\text{disk}} - 8.376 \quad (2)$$

for 157 FSRQs, and

$$\log P_{\text{rad}} = 0.870 \log L_{\text{disk}} + 5.822 \quad (3)$$

for 60 BL Lac objects. These are shown in Figure 4.

Since the disk luminosity can be calculated from the broad-line luminosity $L_{\text{disk}} = 10L_{\text{BLR}}$ (Calderone et al. 2013), and it is supposed that $L_{\text{jet}}^{\text{bol}} = L_{\gamma}$ as it did in Ghisellini et al. (2014), see also Xiong & Zhang (2014), then Equations (1) and (2) give

$$\log \delta = 0.5(\log L_{\gamma} - 1.178 \log L_{\text{BLR}} + 8.004) \quad (4)$$

for FSRQs, and Equations (1) and (3) give

$$\log \delta = 0.5(\log L_{\gamma} - 0.87 \log L_{\text{BLR}} - 6.266) \quad (5)$$

for BL Lac objects.

In this way, we can get the Doppler factor, δ , for a source with known γ -ray luminosity and broad-line luminosity. For the present 350 Fermi blazars, the obtained Doppler factor δ , listed in Table 3, is in a range of 0.35–85.66 with an average value of $\langle \delta \rangle = 12.54$ for the whole sample. When we considered FSRQs and BL Lac objects separately, the corresponding range and average values are $\delta = 0.61$ –85.66 with $\langle \delta \rangle = 13.16$ for FSRQs and $\delta = 0.35$ –53.57 with $\langle \delta \rangle = 10.25$ for BL Lac objects. See Figure 5 for the distributions of the Doppler factors. For comparison, we also collected the Doppler factor from Ghisellini et al. (2014), Chen (2018), and Liodakis et al. (2018) in Table 3.

4. Discussions

4.1. Broad-line Luminosity

During the process of calculating and fitting broad-line luminosity, there are some issues we need to be concerned with, such as the airmass extinction, contamination of host galaxies, and Fe II emission lines. We do not correct the airmass because the airmass correction of the spectra has been done by the SDSS. For the second issue, the light entering into the aperture of the telescope instrument is mainly composed of two parts, one derived from the central AGN, another from the host galaxies surrounding the AGN, especially for type 2 AGNs. One outstanding question is how to determine the amount of the stellar light is from AGNs and host galaxies, and separate them. Some attempts try to separate these two components by principal component analysis (PCA) originates from Connolly et al. (1995). This issue may largely affect the continua, but not broad emission lines that mostly originate from AGNs. For this reason, doing PCA is then unnecessary for measuring the broad emission lines. Another issue is that Fe II emission lines are a prominent feature for AGNs and arise in the optical band, which may have an influence on the continuum and emission-line measurements. A global inspection from the results of the fitting of broad-line emissions shows that Fe II emission lines have a remote effect on the spectra within a range from 4000–5500 Å. Likewise, the impacts of Fe II emission lines were ignored. In this way, we obtained the broad-line luminosity for 50 Fermi blazars, their corresponding logarithm, $\log L_{\text{BLR}} (\text{erg s}^{-1})$, is in a range of 41.82–45.2 with a mean value 44.39. For the whole 350 Fermi blazars, we found that the broad-line luminosity is in a range of $41.7 (\text{erg s}^{-1}) < \log L_{\text{BLR}} < 46.43 (\text{erg s}^{-1})$ with a mean value of $\langle \log L_{\text{BLR}} \rangle = 44.52 (\text{erg s}^{-1})$. For FSRQs and BL Lac object subclasses, we have $\langle \log L_{\text{BLR}} \rangle = 44.69 (\text{erg s}^{-1})$ for FSRQs and $\langle \log L_{\text{BLR}} \rangle = 43.91 (\text{erg s}^{-1})$ for BL Lac objects. The broad emission-line luminosity in FSRQs is higher than that in BL Lac objects.

⁶ https://astrostatistics.psu.edu/statcodes/sc_regression.html

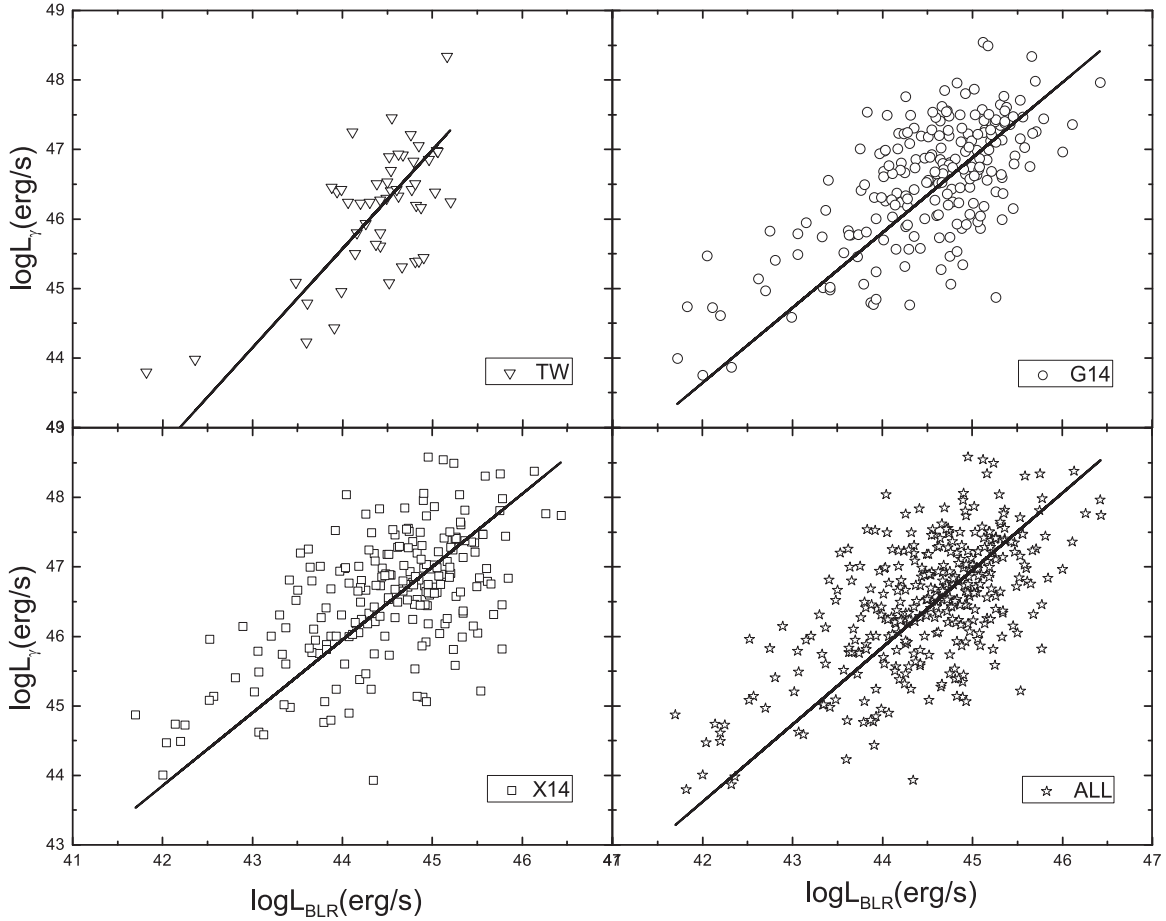


Figure 3. Plot of γ -ray luminosity vs. broad-line luminosity. Different symbols correspond to the different populations, as labeled. Top left: $\log L_\gamma$ vs. $\log L_{\text{BLR}}$ for the 50 new blazars we calculated. Top right: $\log L_\gamma$ vs. $\log L_{\text{BLR}}$ for the sources from Ghisellini et al. (2014) (G14). Bottom left: $\log L_\gamma$ vs. $\log L_{\text{BLR}}$ for the sources from Xiong & Zhang (2014) (X14). Bottom right: $\log L_\gamma$ vs. $\log L_{\text{BLR}}$ for a whole sample of 350 blazars (ALL) in this work.

Table 2
Linear Regression Results from Fitting

Y (1)	X (2)	Source (3)	N (4)	$a \pm \Delta a$ (5)	$b \pm \Delta b$ (6)	r (7)	p (8)
$\log L_\gamma$	$\log L_{\text{BLR}}$	TW	50	1.42 ± 0.17	-16.91 ± 7.67	0.68	<0.0001
$\log L_\gamma$	$\log L_{\text{BLR}}$	G14	217	1.08 ± 0.05	-1.72 ± 2.22	0.67	<0.0001
$\log L_\gamma$	$\log L_{\text{BLR}}$	X14	217	1.05 ± 0.05	-0.25 ± 2.14	0.60	<0.0001
$\log L_\gamma$	$\log L_{\text{BLR}}$	ALL	350	1.11 ± 0.04	-3.00 ± 1.82	0.62	<0.0001
$\log L_\gamma$	$\log \delta$	L18	209	1.77 ± 0.13	44.48 ± 0.18	0.42	<0.0001
$\log L_\gamma$	$\log \delta$	G14	217	8.69 ± 1.19	37.01 ± 1.3	0.37	<0.0001
$\log L_\gamma$	$\log \delta$	C18	283	1.55 ± 0.21	44.80 ± 0.23	0.18	0.002
$\log L_\gamma$	$\log \delta$	ALL	350	2.14 ± 0.10	44.46 ± 0.11	0.56	<0.0001

Note. Column definitions: (1) dependent variable (γ -ray luminosity); (2) independent variable (BLR luminosity or Doppler factor); (3) references for independent variables: TW: broad-line region luminosity calculated in this work for the 50 new sources; G14: Ghisellini et al. (2014); X14: Xiong & Zhang (2014); ALL: 350 sources with broad-line luminosity in this work; (4) number of sources; (5) slope; (6) intercept; (7) correlation coefficient; (8) probability.

4.2. Correlations

There is correlation evidence between jet power and accretion luminosity (Maraschi & Tavecchio 2003; Punsly & Tingay 2006; Celotti & Ghisellini 2008; Ghisellini et al. 2010, 2014). In this work, we enlarge the Fermi blazar sample for the purpose of revisiting the correlation between jet power (presented as γ -ray luminosity) and the accretion luminosity (presented as broad-line luminosity). When the method of OLS

regression (Feigelson & Babu 1992) is adopted to the linear correlation analysis, it is found to be strongly correlated with broad-line luminosity as $\log L_\gamma = (1.11 \pm 0.04)\log L_{\text{BLR}} - (3.00 \pm 1.82)$ with a correlation coefficient $r = 0.62$ and a chance probability $p < 0.0001$ for 350 sources in this work, which is shown in the bottom right panel of Figure 3. For the sources in the literature (Ghisellini et al. 2014; Xiong & Zhang 2014), we obtained $\log L_\gamma = (1.08 \pm 0.05)\log L_{\text{BLR}} - (1.72 \pm 2.22)$

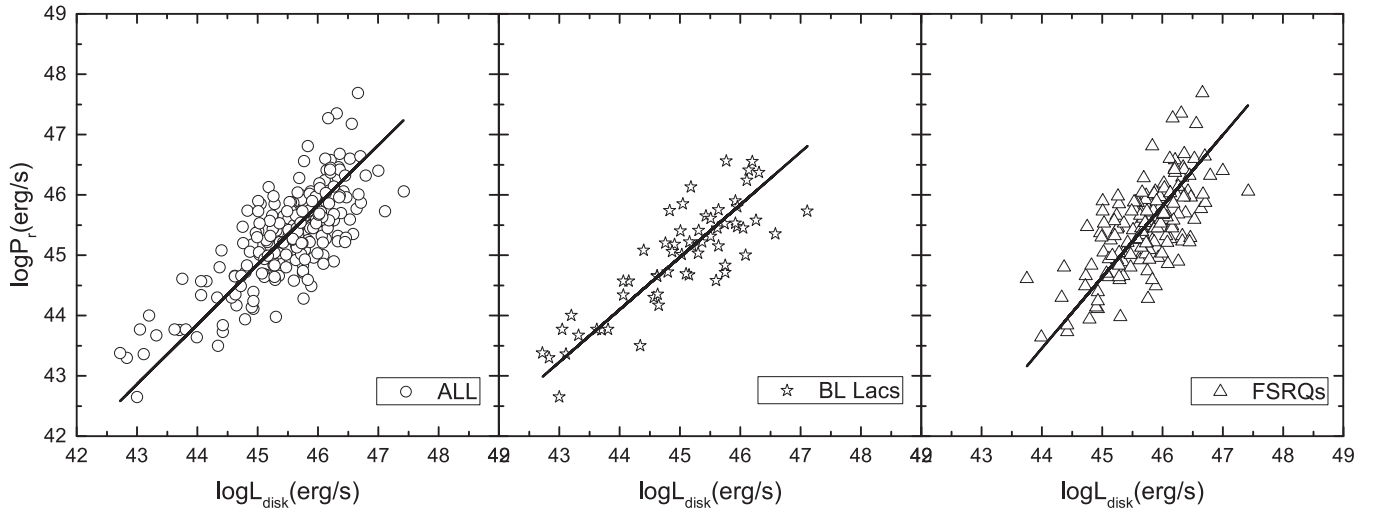


Figure 4. Plot of radiative jet power vs. disk luminosity. Different symbols correspond to the different populations, as labeled. Left panel: circular symbols represent the whole sample of 217 blazars with fitting: $\log P_{\text{rad}} = 0.990 \log L_{\text{disk}} + 0.291$ with $r = 0.77$ and $p < 0.0001$. Middle panel: star symbols represent 60 BL Lac objects with fitting: $\log P_{\text{rad}} = 0.870 \log L_{\text{disk}} + 5.822$ with $r = 0.85$ and $p < 0.0001$. Right panel: triangle symbols represent 157 FSRQs with fitting: $\log P_{\text{rad}} = 1.178 \log L_{\text{disk}} - 8.376$ with $r = 0.67$ and $p < 0.0001$. The linear regression lines are fitted by a symmetric regression line (OLS bisector).

Table 3
List of Sources with Doppler Factors

Name (1)	Other Name (2)	δ^{ALL} (3)	δ^{G14} (4)	δ^{L18} (5)	δ^{C18} (6)
4FGL J0004.4-4737	PKS 0002-478	10.82	14		12.3
4FGL J0011.4+0057	[VV2006] J001130.4+005751	6.13	13	11.03	
4FGL J0014.1+1910	ICRF J001356.3+191041	5.99	11		
4FGL J0016.5+1702	0015+1700	2.36	12		
4FGL J0016.2-0016	S3 0013-00	8.21		18.94	6.7
4FGL J0017.5-0514	PMN 0017-0512	3.89	12	12.02	5
4FGL J0023.7+4457	B3 0020+446	10.31	15	19.63	7.6
4FGL J0023.7+4457	7C 002055.00+444012.00	10.31	15		
4FGL J0024.7+0349	GB6 J0024+0349	5.44	13		25.5
3FGL J0042.0+2318	QSO B0039+230	9.49	13		17.8
4FGL J0043.8+3425	GB6 J0043+3426	36.42	14		12.6

Note. Column definitions: (1) name; (2) other name; (3) the Doppler factor calculated from this work (δ^{ALL}); (4) the Doppler factor from Ghisellini et al. (2014) (δ^{G14}); (5) the Doppler factor from Liodakis et al. (2018) (δ^{L18}); (6) the Doppler factor from Chen (2018) (δ^{C18}).

(This table is available in its entirety in machine-readable form.)

with $r = 0.67$ and $p < 0.0001$ for 217 sources from Ghisellini et al. (2014), and $\log L_{\gamma} = (1.05 \pm 0.05) \log L_{\text{BLR}} - (0.25 \pm 2.14)$ with $r = 0.60$ and $p < 0.0001$ for 217 sources from Xiong & Zhang (2014). It seems that the correlation results obtained for the present 350 sources, the 217 sources from Ghisellini et al. (2014), and the 217 sources from Xiong & Zhang (2014) are consistent with each other. The corresponding results are listed in Table 2 and shown in Figure 3.

The correlation in Figure 3 is significant. However, as stated in a paper by Kendall & Stuart (1979), a luminosity–luminosity correlation can be a distance-driven effect from a common dependence on redshift. To remove the effect of redshift on the correlation between γ -ray luminosity and the broad-line luminosity, we adopted the partial correlation analysis (Padovani 1992), and got a partial correlation coefficient $r_{LL,z} = 0.18$ and a chance probability $p = 0.0008$ for the whole sample, which suggests that the correlation between γ -ray luminosity and broad-line luminosity still exists after removing the redshift effect.

The beaming effect has been discussed for the Fermi-detected blazars (Kovalev et al. 2009; Arshakian et al. 2010;

Fan et al. 2017). From the present work, we find that γ -ray luminosity is also correlated with the Doppler factor as $\log L_{\gamma} = (2.14 \pm 0.10) \log \delta + (44.46 \pm 0.11)$ with a correlation coefficient $r = 0.56$ and a chance probability $p < 0.0001$ also by the OLS method. We also investigated the correlation between the γ -ray luminosity and the Doppler factor using the Doppler factors from Ghisellini et al. (2014) (here $\delta \sim \Gamma$), Chen (2018), and Liodakis et al. (2018); positive correlations are shown in Figure 6 and listed in Table 2.

It is found from Figure 6 that even though the Doppler factors were from different methods, the γ -ray luminosity is positively correlated with the Doppler factors, suggesting that the γ -rays are beamed. The Doppler factors used in Figure 6 are from different methods, listed as follows. In Liodakis et al. (2018), the Doppler factors were estimated from the equipartition brightness temperature, observed variability brightness temperature, and redshift based on the radio regime. The equipartition brightness temperature of all populations was considered the same as the mean value from a Gaussian distribution of FSRQs. In Ghisellini et al. (2014), the Doppler

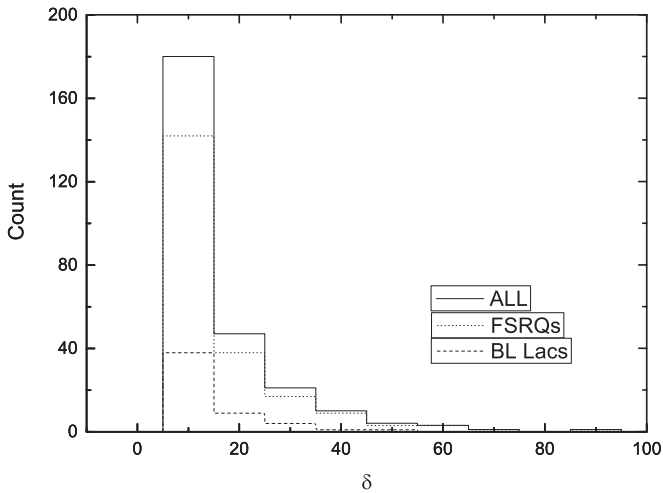


Figure 5. Distributions of the Doppler factor: the solid line is for all sources, the dotted line is for FSRQs, and the dashed line is for BL Lac objects.

factors are from SED fitting, depending on the model. While in Chen (2018), the Doppler factors were estimated from peak luminosity and frequency, both in the synchrotron bump and inverse Compton bump, timescales, and curvature of the observed SED of the synchrotron component, where the timescale is assumed as $\Delta t/(1+z) \approx 1$ day. In this work, we estimate the Doppler factor using both γ -ray luminosity and BLR luminosity based on the γ -ray band. For one source, different methods will give a different Doppler factor value, therefore, the correlation between γ -ray luminosity and the Doppler factor is different from the other Doppler estimation methods.

4.3. Doppler Factor

The Doppler factor is an important parameter for blazars, but it is hard to determine accurately. As we mentioned in the Introduction, there are some methods proposed for the estimation (Ghisellini et al. 2014; Chen 2018; Lioudakis et al. 2018). In terms of the estimation for the SED modeling for the Doppler factor, a general assumption is $\delta \approx \Gamma$ for blazars, a narrow distribution of the Doppler factor peaking at $\delta = \Gamma \sim 13 \pm 1.4$ was found through SED modeling for a sample of 217 blazars (Ghisellini et al. 2014). Chen (2018) obtained a Doppler factor for 999 sources, the values in a range of 1–99.5 give a mean value of 17.61. Besides, another way for estimating the variability of the Doppler factor is based on the radio regime, as shown in recent work by Lioudakis et al. (2018), by giving the constraints on variability brightness temperature for 878 sources (670 FSRQs, 118 BL Lac objects, 33 radio galaxies and 57 uncertain sources), resulting in a median value of $\delta \approx 14$ and a median value of $\Gamma \approx 17$ for 878 sources. In this work, based on the correlation between the radiation power of the jet and the broad-line luminosity, and between radiation power and the bolometric luminosity of the jet (Ghisellini et al. 2014), we can compute a Doppler factor when we take the γ -ray luminosity as the jet bolometric luminosity. Hence, we can estimate the Doppler factor using the γ -ray luminosity and broad-line luminosity. This is a new method to estimate the Doppler factor for Fermi blazars.

In Table 3, we also collected Doppler factors from Ghisellini et al. (2014), Chen (2018), and Lioudakis et al. (2018) for sources contained in this work, and made a comparison for

Table 4
Parameters of δ for Common Sources

Source (1)	ALL (2)	G14 (3)	L18 (4)	C18 (5)
Minimum	0.35	5	0.23	1.3
Maximum	85.66	18	88.44	94
Median	9.16	13	17.24	13.3
Mean	12.54	12.77	19.46	16.06
Mean for FSRQs	13.16	12.88	20.00	13.87
Mean for BL Lac objects	10.25	12.44	16.68	27.33

Note. Column definitions: (1) statistical parameters; (2) parameter for the whole sample (350 sources) (ALL); (3) parameter for Ghisellini et al. (2014) (G14); (4) parameter for Lioudakis et al. (2018) (L18); (5) parameter for Chen (2018) (C18).

common sources. We noted that the resulting δ in our sample is mainly distributed within a range from 1 to 80, except for one FSRQ and three BL Lac objects whose Doppler factors are smaller than 1 (FSRQ 4FGLJ1229.0+0202 ($\delta = 0.61$); BL Lac objects 4FGLJ0747.2+4529 ($\delta = 0.35$), 4FGLJ1014.8+2257 ($\delta = 0.80$), and 4FGLJ2148.6+0652 ($\delta = 0.74$), and one FSRQ whose Doppler factor is greater than 80 (4FGLJ0958.7+6534 ($\delta = 85.66$)). The mean values of the Doppler factors are $\delta = 13.16$ and $\delta = 10.25$ for FSRQs and BL Lac objects, respectively.

For comparison, we found 217 sources from Ghisellini et al. (2014) that have a mean value of $\delta = 12.77$ in a range of $5 < \delta < 18$, their mean values are $\delta = 12.88$ and $\delta = 12.44$ for FSRQs and BL Lac objects, respectively.

There are 210 common sources with Chen (2018), which show a range of $1.3 < \delta < 94$ with a mean value of $\delta = 16.06$, their mean values are $\delta = 13.87$ and $\delta = 27.33$ for FSRQs and BL Lac objects, respectively. There is no source showing δ to be less than 1 but there are three sources showing δ to be greater than 80 (83, 86.3, 94).

There are 283 common sources with Lioudakis et al. (2018), which are in a range of $0.23 < \delta < 88.44$ with a mean value of $\delta = 19.46$, their mean values are $\delta = 20.00$ and $\delta = 16.68$ for FSRQs and BL Lac objects, respectively. One source shows its Doppler factor to be smaller than 1 ($\delta = 0.23$), and one source shows its Doppler factor to be greater than 80 ($\delta = 88.44$). The Doppler factors in Ghisellini et al. (2014), Lioudakis et al. (2018), and our work show that BL Lac objects have, on average, smaller Doppler factors than FSRQs, and while it is the reverse for those from Chen (2018), we think that the assumption of $\Delta t/(1+z) = 1$ day is not true for all the sources. The compared parameters are listed in Table 4.

The large amplitude variability for γ -ray emission may be larger than two orders of magnitude during the period of flares, and the emission in the γ -ray band may be detected in the high state rather than average state (Ghisellini et al. 2014). If the γ -ray emissions are two orders of magnitude brighter than the values used in the present work, then the Doppler factor will have an enhancement of one order of magnitude according to Equations (4) and (5). Namely, the Doppler factors are a factor of 10 larger than those listed in Table 1. When the γ -ray emissions are fainter than those used in the present work, the Doppler factors will be smaller than those listed in Table 1. In the present work, the Doppler factors for 324 sources are calculated from the γ -ray data in 4FGL while those for the other 26 sources are obtained from the γ -ray data in 1FGL,

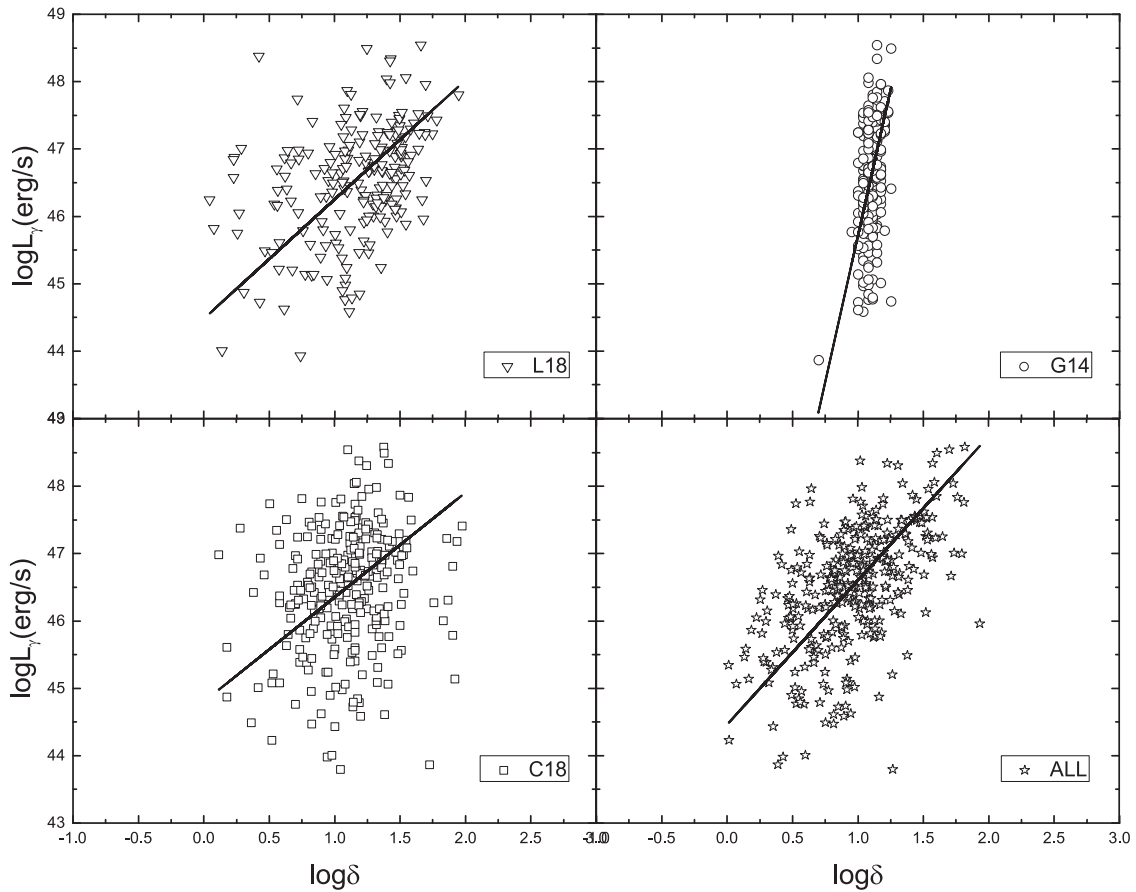


Figure 6. Plot of γ -ray luminosity vs. Doppler factor. Different symbols correspond to the different populations, as labeled. Top left: $\log L_\gamma$ vs. $\log \delta$ for the sources from Liodakis et al. (2018) (L18). Top right: $\log L_\gamma$ vs. $\log \delta$ for the sources from Ghisellini et al. (2014) (G14). Bottom left: $\log L_\gamma$ vs. $\log \delta$ for the sources from Chen (2018) (C18). Bottom right: $\log L_\gamma$ vs. $\log \delta$ for the whole sample in this work (ALL).

2FGL, and 3FGL. Since the γ -ray data in 4FGL are from the last 8 years, their averaged values are smaller than their maximum emissions, so the Doppler factors listed in Table 1 are lower than those obtained from their single-flare data.

5. Conclusions

In this paper, we obtained emission-line luminosity for 50 Fermi blazars by matching SDSS with 3FGL and 4FGL and compiled emission-line luminosity for 300 Fermi blazars from the literature and got a sample of 350 Fermi blazars (275 FSRQs and 75 BL Lac objects). We revisited the correlation between γ -rays and emission-line luminosity, and proposed a new method to estimate the Doppler factor for Fermi blazars. Finally, we estimated the Doppler factor and made linear correlation analysis between the γ -ray luminosity and the Doppler factor, and made Doppler factor comparisons with the available results from the literature.

Our conclusions are as follows:

1. The broad-line emissions from SDSS are obtained for 50 Fermi blazars. The logarithm of their broad-line luminosities are in the range of $41.82\text{--}45.2 \text{ erg s}^{-1}$ with a mean value of 44.39 erg s^{-1} , and we obtained a sample of 350 Fermi sources with broad-line emissions.
2. Doppler factors are found in a range of $\delta = 0.35$ to $\delta = 85.66$ for 350 Fermi blazars. The average values of the Doppler factors are $\delta = 13.16$ and $\delta = 10.25$ for FSRQs and BL Lac objects, respectively. The Doppler

factor in BL Lac objects is, on average, smaller than that in FSRQs, which is consistent with those obtained from Ghisellini et al. (2014) and Liodakis et al. (2018).

3. The γ -ray luminosity is closely correlated with both the broad-line luminosity and the Doppler factor.

We thank the anonymous referee for the useful comments and suggestions. The work is partially supported by the National Natural Science Foundation of China (NSFC 11733001, NSFC U1531245), the Natural Science Foundation of Guangdong Province (2017A030313011; 2019B030302001), and the Astrophysics Key Subjects of Guangdong Province and Guangzhou City. Support was also received from Guangzhou University (2019GDJC-D18).

ORCID iDs

Hubing Xiao  <https://orcid.org/0000-0001-8244-1229>

References

- Abdo, A. A., Ackermann, M., Ajello, M., et al. 2010a, *ApJ*, **715**, 429
 Abdo, A. A., Ackermann, M., Ajello, M., et al. 2010b, *ApJS*, **188**, 405
 Acero, F., Ackermann, M., Ajello, M., et al. 2015, *ApJS*, **218**, 23
 Ackermann, M., Ajello, M., Atwood, W. B., et al. 2015, *ApJ*, **810**, 14
 Aharonian, F. A. 2000, *NewA*, **5**, 377
 Aharonian, F. A. 2002, *MNRAS*, **332**, 215
 Arshakian, T. G., León-Tavares, J., Torrealba, J., & Chavushyan, V. H. 2010, arXiv:1006.2079
 Bentz, M. C., Walsh, J. L., Barth, A. J., et al. 2009, *ApJ*, **705**, 199

- Błażejowski, M., Sikora, M., Moderski, R., & Madejski, G. M. 2000, *ApJ*, **545**, 107
- Blandford, R. D., & Payne, D. G. 1982, *MNRAS*, **199**, 883
- Blandford, R. D., & Rees, M. J. 1978, in *BL Lac Objects*, ed. A. M. Wolfe (Pittsburgh, PA: Univ. Pittsburgh), 328
- Blandford, R. D., & Znajek, R. L. 1977, *MNRAS*, **179**, 433
- Bloom, S. D., & Marscher, A. P. 1996, *ApJ*, **461**, 657
- Calderone, G., Ghisellini, G., Colpi, M., & Dotti, M. 2013, *MNRAS*, **431**, 210
- Cao, X., & Jiang, D. R. 1999, *MNRAS*, **307**, 802
- Capelo, P. R., & Natarajan, P. 2007, *NJPh*, **9**, 445
- Celotti, A., & Ghisellini, G. 2008, *MNRAS*, **385**, 283
- Celotti, A., Padovani, P., & Ghisellini, G. 1997, *MNRAS*, **286**, 415
- Chai, B., Cao, X., & Gu, M. 2012, *ApJ*, **759**, 114
- Chen, L. 2018, *ApJS*, **235**, 39
- Chen, S., Berton, M., La Mura, G., et al. 2018, *A&A*, **615**, A167
- Cheng, K. S., Fan, J. H., & Zhang, L. 1999, *A&A*, **352**, 32
- Connolly, A. J., Szalay, A. S., Bershad, M. A., Kinney, A. L., & Calzetti, D. 1995, *AJ*, **110**, 1071
- Dermer, C. D., & Schlickeiser, R. 1993, *ApJ*, **416**, 458
- Dondi, L., & Ghisellini, G. 1995, *MNRAS*, **273**, 583
- Fan, J. H. 2005, *A&A*, **436**, 799
- Fan, J.-H., Bastieri, D., Yang, J.-H., et al. 2014, *RAA*, **14**, 1135
- Fan, J.-H., Huang, Y., He, T.-M., et al. 2009, *PASJ*, **61**, 639
- Fan, J. H., Tao, J., Liu, Y., et al. 2018, *AJ*, **155**, 90
- Fan, J. H., Xie, G. Z., & Bacon, R. 1999, *A&AS*, **136**, 13
- Fan, J.-H., Yang, J.-H., Liu, Y., & Zhang, J.-Y. 2013, *RAA*, **13**, 259
- Fan, J. H., Yang, J. H., Liu, Y., et al. 2016, *ApJS*, **226**, 20
- Fan, J. H., Yang, J. H., Xiao, H. B., et al. 2017, *ApJL*, **835**, L38
- Fan, Z., Cao, X., & Gu, M. 2006, *ApJ*, **646**, 8
- Feigelson, E. D., & Babu, G. J. 1992, *ApJ*, **397**, 55
- Francis, P. J., Hewett, P. C., Foltz, C. B., et al. 1991, *ApJ*, **373**, 465
- Ghisellini, G., Padovani, P., Celotti, A., & Maraschi, L. 1993, *ApJ*, **407**, 65
- Ghisellini, G., & Tavecchio, F. 2010, *MNRAS*, **409**, L79
- Ghisellini, G., Tavecchio, F., Foschini, L., et al. 2010, *MNRAS*, **402**, 497
- Ghisellini, G., Tavecchio, F., Maraschi, L., Celotti, A., & Sbarrato, T. 2014, *Natur*, **515**, 376
- Kaspi, S., Maoz, D., Netzer, H., et al. 2005, *ApJ*, **629**, 61
- Kaspi, S., Smith, P. S., Netzer, H., et al. 2000, *ApJ*, **533**, 631
- Kendall, M., & Stuart, A. 1979, *The Advanced Theory of Statistics*. Vol. 2: Inference and Relationship (London: Griffin)
- Komatsu, E., Smith, K. M., Dunkley, J., et al. 2011, *ApJS*, **192**, 18
- Kovalev, Y. Y., Aller, H. D., Aller, M. F., et al. 2009, *ApJL*, **696**, L17
- Lähteenmäki, A., & Valtaoja, E. 1999, *ApJ*, **521**, 493
- Liodakis, I., Hovatta, T., Huppenkothen, D., et al. 2018, *ApJ*, **866**, 137
- Liu, Y., Jiang, D. R., & Gu, M. F. 2006, *ApJ*, **637**, 669
- Maraschi, L., Ghisellini, G., & Celotti, A. 1992, *ApJL*, **397**, L5
- Maraschi, L., & Tavecchio, F. 2003, *ApJ*, **593**, 667
- Mattox, J. R., Bertsch, D. L., Chiang, J., et al. 1993, *ApJ*, **410**, 609
- Padovani, P. 1992, *A&A*, **256**, 399
- Punsly, B., & Tingay, S. J. 2006, *ApJL*, **640**, L21
- Sbarrato, T., Ghisellini, G., Maraschi, L., & Colpi, M. 2012, *MNRAS*, **421**, 1764
- Schlafly, E. F., & Finkbeiner, D. P. 2011, *ApJ*, **737**, 103
- Shaw, M. S., Romani, R. W., Cotter, G., et al. 2012, *ApJ*, **748**, 49
- Shen, Y., Richards, G. T., Strauss, M. A., et al. 2011, *ApJS*, **194**, 45
- Sikora, M., Begelman, M. C., & Rees, M. J. 1994, *ApJ*, **421**, 153
- The Fermi-LAT Collaboration 2019, arXiv:1905.10771
- Urry, C. M. 1998, *AdSpR*, **21**, 89
- Urry, C. M., & Padovani, P. 1995, *PASP*, **107**, 803
- von Montigny, C., Bertsch, D. L., Chiang, J., et al. 1995, *ApJ*, **440**, 525
- Wang, J.-M., Luo, B., & Ho, L. C. 2004, *ApJL*, **615**, L9
- Xiong, D. R., & Zhang, X. 2014, *MNRAS*, **441**, 3375
- York, D. G., Adelman, J., Anderson, J. E., Jr., et al. 2000, *AJ*, **120**, 1579